

Chirped-beam two-stage free-electron laser for high-power femtosecond x-ray pulse generation

Carl B. Schroeder,* Claudio Pellegrini, and Sven Reiche

Department of Physics and Astronomy, University of California, Los Angeles, California 90095

John Arthur and Paul Emma

Stanford Linear Accelerator Center, Stanford University, Stanford, California 94309

Received November 9, 2001; revised manuscript received March 5, 2002

A method for generating femtosecond-duration x-ray pulses with a free-electron laser is presented. This method uses an energy-chirped electron beam propagating through an undulator to produce a frequency-chirped x-ray pulse by self-amplified spontaneous emission. A short temporal pulse is created by use of a monochromator to select a narrow radiation bandwidth. A second undulator is used to amplify the short-duration radiation. The radiation characteristics produced by a chirped-beam two-stage free-electron laser are calculated, and the performance of the chirped-beam two-stage option for the Linac Coherent Light Source is considered. © 2002 Optical Society of America

OCIS codes: 140.2600, 340.7480, 320.1590, 320.2250, 230.1480.

1. INTRODUCTION

A single-pass free-electron laser (FEL) has the ability to extend the energy range of lasers into the x-ray regime.¹ The Linac Coherent Light Source (LCLS) is a proposal² to construct a single-pass FEL that generates x rays through self-amplified spontaneous emission³ (SASE). As described in this paper, a SASE-FEL, such as the LCLS, can be modified to produce short-duration (femtosecond) radiation. Atomic structural dynamics, e.g., chemical reactions, phase transitions, and surface processes, are driven by the motion of atoms on the time scale of the atomic vibrational period (≥ 100 fs). Since x rays are effective structural probes, development of a source of high-brightness femtosecond x rays would be an important tool for studying the structural dynamics of materials on the fundamental time scale for atomic motion.

The proposed scheme for short-duration radiation generation is based on frequency chirping the radiation pulse. An energy-chirped electron beam is injected into an undulator. The FEL operates in the high-gain linear regime of amplification and produces frequency-chirped radiation with the usual SASE properties.⁴ After the undulator, the radiation is passed through a monochromator, which transmits a narrow bandwidth. Since the radiation frequency is correlated to the longitudinal position within the beam, a short temporal radiation pulse will be transmitted through the monochromator. We consider using a second undulator to amplify the short-pulse radiation. A chicane can be used to delay the electron beam, compensating for the path delay introduced in the radiation pulse by the monochromator and allowing the radiation to recombine with the electron beam at the entrance to the second undulator. The second undulator

acts as a FEL amplifier and amplifies the short-pulse radiation to saturation. Figure 1 illustrates the basic schematic of a chirped-beam two-stage FEL.

The chirped-beam two-stage FEL offers two major advantages over the standard single-pass SASE-FEL. First, it provides control of the radiation-pulse duration and allows the possibility of producing femtosecond radiation pulses. The short-duration pulse will reach saturation in the second undulator and therefore has the same peak power as the standard single-pass SASE-FEL. Second, it provides stability of the shot-to-shot fluctuations in the central wavelength due to shot-to-shot fluctuations in the mean electron-beam energy. The fluctuations in the mean electron-beam energy are caused by jitter throughout the linear accelerator (linac), which accelerates the electron beam before the first undulator.

The seeding of the second undulator has many benefits compared with a single undulator followed by x-ray optics. By seeding the radiation in a second undulator (FEL amplifier), any power loss in the monochromator is recovered in the FEL amplifier. The shot-to-shot radiation-intensity fluctuations after the monochromator are reduced, owing to operation of the FEL amplifier in the nonlinear regime. Since the peak power after the first undulator is much less than the saturation power, the damage to optical elements of the monochromator is reduced. The monochromator will absorb the spontaneous synchrotron radiation power from the first undulator; therefore the total spontaneous synchrotron radiation power at the exit of the second undulator will be less than the standard single undulator SASE-FEL designed to reach saturation. Growth of the uncorrelated energy spread in the electron beam due to longitudinal resistive-wall and surface-roughness wake fields can degrade the

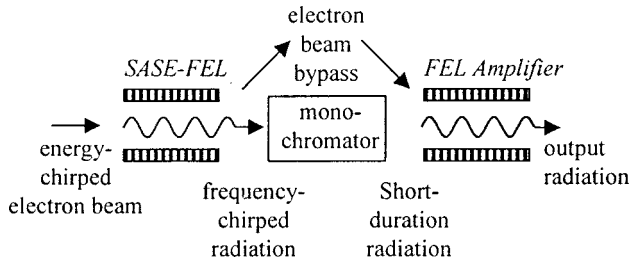


Fig. 1. Schematic of chirped-beam two-stage FEL for short-duration x-ray generation.

Table 1. Linac Coherent Light Source Free-Electron Laser Parameters

Radiation wavelength	1.5 Å
Electron-beam energy	14.3 GeV
FEL parameter	5×10^{-4}
Undulator type	planar
Undulator period	3 cm
Peak undulator field	1.32 T
Undulator parameter	3.7
Repetition rate	120 Hz

performance of the FEL.² These undulator wake-field effects can be mitigated by staging, effectively reducing the undulator length.

The staged two-undulator scheme is similar to proposals to develop a monochromatic x-ray laser,^{5,6} where the desired radiation is selected and seeded into subsequent undulators for coherent amplification. Here we are primarily interested in short-duration x-ray pulse generation and not in monochromatization, although short-pulse generation by this method can result in improved temporal coherence.

The discussion throughout this paper is focused on the parameters for the LCLS.² The basic LCLS FEL parameters are listed in Table 1.

2. RADIATION CHARACTERISTICS

The radiation wavelength λ of a FEL depends on the beam energy measured in rest mass units γ as

$$\lambda = \frac{\lambda_u}{2\gamma^2} (1 + K_{\text{ave}}^2), \quad (1)$$

where λ_u is the undulator period and K_{ave} is the average normalized vector potential of the undulator field. Therefore chirping the electron beam (i.e., providing an energy spread that is correlated to the longitudinal position of the electrons within the beam) before the beam enters the first undulator allows control of the frequency distribution of the radiation pulse generated in the undulator. Chirping of the electron beam may be accomplished by acceleration of the electron bunch in a linac at an off-crest phase of the accelerating field. We will consider a linear energy chirp on the electron beam such that

$$\frac{\delta\gamma}{\gamma} = \alpha \frac{l}{L_b}, \quad (2)$$

where L_b is the full width at half-maximum (FWHM) bunch length and l is the longitudinal deviation from the beam centroid. Due to the resonant condition Eq. (1), the energy chirp Eq. (2) will produce a correlated frequency chirp of the resonant radiation $\delta\omega/\omega \approx 2\delta\gamma/\gamma = 2\alpha l/L_b$.

The temporal structure of a radiation pulse produced by a SASE-FEL³ will consist of randomly distributed spikes (wave packets) of root-mean-square (rms) duration (coherence length) σ_τ , determined by the rms FEL bandwidth σ_ω ,

$$\sigma_\tau = \frac{1}{2\sigma_\omega} \approx \frac{\lambda}{4\pi\rho c} (N_u\rho)^{1/2}, \quad (3)$$

where ρ is the FEL parameter,³ $\lambda/4\pi\rho$ is the cooperation length, and N_u is the number of undulator periods. The FEL process saturates at $N_u \approx 1/\rho$. There is full longitudinal coherence of the radiation within one spike but no phase correlation between spikes. The number of spikes in the distribution is approximately given by $N_s \approx L_p/(2\pi c\sigma_\tau)$, where L_p is the FWHM radiation-pulse length. For the LCLS, the cooperation length is 48 nm, and the rms spike duration at saturation is $\sigma_\tau \sim 0.16$ fs.

The width of the spectral distribution of the SASE radiation will be determined by the frequency chirp, provided the frequency chirp is larger than the FEL bandwidth (i.e., $\delta\omega = 2\alpha\omega > \sigma_\omega$). The spectral distribution will also consist of N_s random spikes (modes). For large chirp $\delta\omega = 2\alpha\omega \gg N_s\sigma_\omega$, the spectral width of each mode is the FEL bandwidth $\Delta\omega \sim \sigma_\omega$. For LCLS, the rms FEL bandwidth is $\sigma_\omega/\omega \sim 10^{-4}$. For the unchirped case $\delta\omega = 2\alpha\omega \ll \sigma_\omega$, the spectral width of each mode is determined by the Fourier-transform-limited bandwidth $\Delta\omega \sim c/L_b$. For the LCLS, $\lambda/L_b \approx 2 \times 10^{-6}$.

The growth of the radiation due to the collective FEL instability in the high-gain regime will be modified by the energy chirp on the electron beam. The coupled Maxwell-Boltzmann equations describing the FEL instability are solved in Appendix A. Linear analysis of the generalized FEL dispersion relation [Eq. (19) of Appendix A] indicates that the increase in gain length will be small if the energy chirp over one slippage length is small, $\alpha \ll L_b\rho^2/\lambda$. As shown in Appendix A, the leading order correction to the one-dimensional (1D) gain length can be approximated as

$$L_g \approx \frac{\lambda_u}{4\pi\rho\sqrt{3}} \left[1 + \frac{1}{9} \left(\frac{\alpha\lambda}{\rho^2 L_b} \right)^2 \right]. \quad (4)$$

Equation (4) indicates that, to lowest order in the linear regime, the gain length is independent of the sign of the electron-beam energy chirp. Note that $\alpha\lambda/(L_b\rho^2) \sim 10^{-2}$, for LCLS parameters with $\alpha = 5 \times 10^{-3}$.

A. Femtosecond Pulse Generation

A monochromator may be used to select the pulse duration due to the correlation between frequency and longitudinal position introduced in the radiation. The rms pulse length of the transmitted radiation will be approximately

$$\sigma_z \approx \frac{L_b}{2\alpha} \left(\frac{\sigma_m}{\omega} \right), \quad (5)$$

where σ_m is the rms frequency bandwidth of a Gaussian-line monochromator. Transmission through the monochromator will produce some intrinsic spreading of the pulse, and the minimum pulse duration that may be selected by this method is limited by the properties of wave packets (uncertainty principle) $(\sigma_z/c)\sigma_m \geq 1/2$. The minimum pulse duration that can be selected by this method is $\sigma_{\min} = [L_b/(2\alpha c\omega)]^{1/2}$ with a monochromator bandwidth of $\sigma_m/\omega = [\alpha\lambda/(2\pi L_b)]^{1/2}$. As a numerical example, if we consider a 0.5% chirp ($\alpha = 5 \times 10^{-3}$) over the LCLS beam ($L_b/c = 233$ fs) and a monochromator with rms frequency bandwidth $\sigma_m/\omega = 1.3 \times 10^{-4}$, then a rms pulse duration of $\sigma_z/c \approx 3.0$ fs (or FWHM pulse duration of $L_p/c \approx 7.1$ fs) is transmitted. The minimum rms pulse duration that can be selected by this method by use of the LCLS beam with a 0.5% chirp is $\sigma_z/c \approx 1.4$ fs with a rms monochromator frequency bandwidth of $\sigma_m/\omega \approx 4.1 \times 10^{-5}$. Such a pulse would have complete longitudinal coherence.

The fluctuations in the radiation power after the monochromator will approximately obey a negative-binomial probability distribution characteristic of multimode thermal radiation.^{7,8} If we choose the monochromator bandwidth to be larger than the spectral interval of coherence, i.e., $N_s > 1$, the relative rms power fluctuations after the monochromator will be

$$\frac{\sigma_P}{P} \approx \left(\frac{2\pi c \sigma_\tau}{L_p} \right)^{1/2}. \quad (6)$$

Note that σ_τ is a function of the undulator length as shown in Eq. (3), and the FWHM pulse length L_p is determined by the chirp (α/L_b) and the monochromator bandwidth. As Eq. (6) indicates, the short-pulse selection will result in large radiation power fluctuations after the monochromator.

B. Frequency Stabilization

We expect shot-to-shot fluctuations in the mean electron-beam energy due to jitter throughout the linac. This will lead to shot-to-shot fluctuations in the frequency of the radiation. Provided the correlated energy chirp is larger than the shot-to-shot mean energy fluctuations, the resulting frequency-chirped radiation pulse will span the expected deviation owing to the jitter. This will allow the monochromator to select the desired frequency and therefore stabilize the shot-to-shot jitter. For LCLS, the expected mean beam energy jitter from the linac is 0.1%. Stabilizing the frequency jitter by this method will introduce arrival-time jitter for the short-duration radiation pulse.

3. LINAC COHERENT LIGHT SOURCE CASE

In this section we investigate the requirements for each component of the chirped-beam two-stage FEL, and, as a numerical example, we consider the performance of the chirped-beam two-stage FEL using the LCLS design parameters.²

A. Self-Amplified Spontaneous-Emission Free-Electron Laser

The first undulator operates as a SASE-FEL, starting from noise in the beam and amplifying the spontaneous emission. The input electron-beam and output-radiation parameters for the first undulator are listed in Table 2. The first undulator is required to be of sufficient length such that the output power transmitted through the monochromator and seeded into the second undulator is much larger than the effective power of the electron-beam bunching due to shot noise. Since we propose to reuse the electron beam in the second undulator, the length of the first undulator is limited by the growth of the uncorrelated slice energy spread. In the exponential regime of amplification, the uncorrelated rms slice energy spread in the electron beam increases during the SASE process as

$$\frac{\sigma_\gamma}{\gamma} \approx \rho \left(\frac{P_1}{P_{\text{sat}}} \right)^{1/2}, \quad (7)$$

where P_1 is the output radiation power emitted in the first undulator and P_{sat} is the saturation power. The growth rate of the amplification becomes negligible when $\sigma_\gamma/\gamma \geq \rho$. Therefore in order to reuse the electron beam in the second undulator and have significant amplification, the first undulator must terminate before saturation. We will consider terminating the first undulator such that $P_1/P_{\text{sat}} \approx 10^{-3}$. For LCLS parameters, this corresponds to a first-undulator length of $L_1 = 43.2$ m, with mean output peak radiation power $\langle P_1 \rangle = 13$ MW. Figure 2 shows an example of the temporal structure of the SASE radiation pulse after the first undulator. Figure 2 was generated with GENESIS,⁹ a fully three-dimensional time-dependent FEL simulation code.

B. Monochromator

For 8.3-keV photons ($\lambda = 1.5$ Å), we consider Bragg diffraction in crystals as the method of bandwidth selection. For example, one can consider silicon (Si) or germanium (Ge) crystals. Si (111) crystals have a rms bandwidth of 5.5×10^{-5} and would produce a 3.4-fs FWHM bunch for the LCLS beam with 0.5% energy chirp. Ge (111) crystals have a rms bandwidth of 1.3×10^{-4} and would produce a 7.1-fs FWHM bunch for the LCLS beam with 0.5% energy chirp. Utilizing a four-reflection scheme, the transmitted radiation pulse will remain in the same di-

Table 2. First Undulator ($L_1=43.2$ m) Input Electron-Beam and Output-Radiation Parameters

Input electron beam:	
Peak current	3.4 kA
Bunch duration, FWHM	233 fs
Correlated energy spread	0.5%
Uncorrelated energy spread	0.006%
Output radiation:	
Resonant frequency chirp	1%
Pulse duration, FWHM	233 fs
Mean peak radiation power	13 MW
Coherence length	44 nm
Rayleigh range	40 m

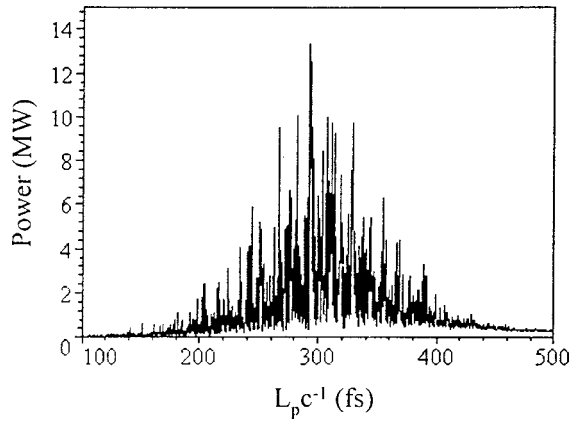


Fig. 2. Temporal structure of SASE radiation pulse after first undulator (SASE-FEL).

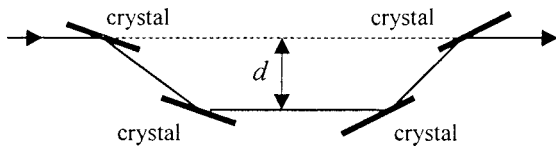


Fig. 3. Schematic of four-reflection crystal monochromator.

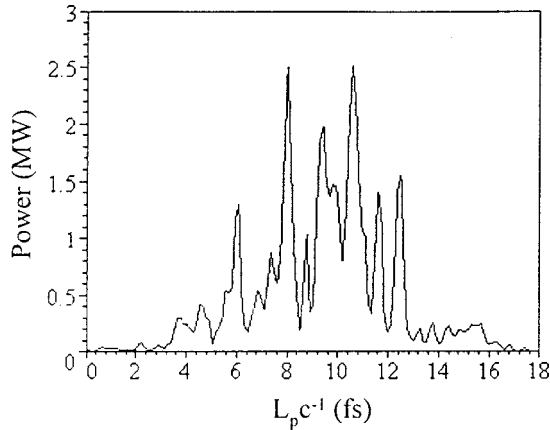


Fig. 4. Temporal structure of radiation pulse shown in Fig. 2 after transmission through a Ge (111) crystal monochromator.

rection and transverse position. Figure 3 illustrates a four-reflection crystal monochromator. The path delay, with respect to the straight path, introduced in the photon beam by the four-reflection crystal monochromator is

$$\Delta L = 2d \tan \theta_B, \quad (8)$$

where θ_B is the Bragg-reflection angle and d is the transverse displacement from the straight path. As Eq. (8) indicates, this method provides tunability of the path delay ΔL by varying the displacement d for a fixed Bragg-reflection angle.

Bragg reflections in perfect crystals typically have reflectivities of approximately 75% within the reflection passband. For the four-reflection scheme, the power transmission through the monochromator would be $\sim 30\%$. For a LCLS x-ray beam with 13-MW peak power, $\sim 3 \mu\text{J}$ is deposited in the monochromator per pulse. This is equivalent to less than 0.005 eV deposited per atom within the volume of the crystal exposed to the incident

beam. This energy deposition per atom (at a repetition rate of 120 Hz) is unlikely to damage the crystal monochromator.

Using a Ge (111) monochromator after the first undulator, with the parameters listed in Table 2, produces a 7.1-fs FWHM pulse after the monochromator. Figure 4 shows the temporal structure of the radiation pulse shown in Fig. 2 after transmission through a four-reflection Ge (111) monochromator.

The choice of monochromator will limit the wavelength tunability of the FEL device. For longer radiation wavelengths, Bragg reflections cannot be achieved in high-quality crystals, such as silicon or germanium, and artificial multilayer monochromators become more attractive.

C. Electron-Beam Bypass

The distance between the two undulators is defined by the parameters of the electron-beam bypass. We can consider a chicane that will match the electron-beam betatron functions from the exit of the first undulator to the entrance of the second undulator and provide a path delay to the electron beam to compensate for the photon-beam path delay induced in the monochromator. An achromatic nonisochronous chicane is desirable because it allows for some compression of the energy-chirped electron beam, providing a larger peak current for coherent amplification in the second undulator. By selecting the nominal frequency in the monochromator and providing equal path delay for both the photon and electron beams, the short-pulse radiation will recombine at the entrance of the second undulator with the resonant electrons.

The input radiation into the second undulator must be much greater than the effective power of bunching at the radiation wavelength in the electron beam. Therefore the electron bunching produced by the FEL interaction in the first undulator should be destroyed in the electron-beam bypass before the second undulator. This demodulation of the electron beam on the scale of the radiation wavelength is easily accomplished by passing the beam through the nonisochronous chicane.

For the LCLS electron-beam parameters, a nonisochronous ($R_{56} = 3.6 \text{ mm}$) chicane of length $L_{\text{by}} = 32.4 \text{ m}$ can be used to provide a path delay for the electron beam of 5 mm with a maximum off-axis displacement of 20.5 cm. For an energy chirp of 0.5%, the beam is compressed $\sim 14\%$ in the chicane.

D. Free-Electron Laser Amplifier

The second undulator operates as a FEL amplifier and is seeded by the radiation pulse selected in the monochromator. The input electron- and photon-beam parameters for the second undulator are listed in Table 3. We require that the mean input radiation power at the entrance of the second undulator dominate over the effective power of the beam shot noise, $\langle P_2 \rangle \gg P_{\text{shot}}$.

The peak input radiation power at the entrance of the second undulator is $P_2 \approx P_1 T_{\text{mono}} T_{\text{diff}} T_{\text{spread}}$, where T_{mono} accounts for attenuation losses in the monochromator, $T_{\text{diff}} = [1 + (L_{\text{by}}/Z_R)^2]^{-1}$ accounts for the power loss between the first and second undulators owing to diffraction of the radiation pulse with Rayleigh range Z_R , and T_{spread} is the peak power reduction due to the spread-

ing of the radiation wave packets in the monochromator. If the chirp is larger than the FEL bandwidth, then the width of the spectral distribution of the SASE radiation field into the monochromator will be determined by the frequency chirp $\delta\omega/\omega = 2\alpha$, and the peak power reduction due to pulse spreading will be $T_{\text{spread}} \approx (L_b/\sigma_z)(\sigma_m/\delta\omega)$. In the regime where the wave-packet spreading due to bandwidth selection in the monochromator is small, Eq. (5) is valid, and $T_{\text{spread}} \approx 1$. If the monochromator bandwidth is much less than the FEL bandwidth, then there will be significant spreading of the radiation wave packets and the peak radiation power will be reduced, $T_{\text{spread}} = \sigma_m/\sigma_\omega$.

For the parameters in Table 2, with a Ge (111) monochromator, the mean radiation power into the second undulator is $\langle P_2 \rangle = 2.5 \text{ MW} \gg P_{\text{shot}} \approx 6.4 \text{ kW}$. Note that if the minimum pulse duration σ_{min} were selected, then $T_{\text{spread}} < 1$, resulting in reduction of the peak radiation power seeding the second undulator and therefore requiring a longer second undulator to reach saturation.

The input-radiation pulse is amplified in the second undulator to saturation. With the compressed LCLS beam, the coherent amplification saturates at $P_{\text{sat}} = 23 \text{ GW}$ after an undulator length of $L_2 = 51.8 \text{ m}$. Table 3 lists the output-radiation characteristics for the chirped-beam two-stage FEL based on LCLS parameters. The output-radiation parameters were calculated with the FEL simulation code GENESIS.⁹ The total length of the system as designed is $L_1 + L_{\text{by}} + L_2 = 127.4 \text{ m}$. Figure 5 shows the mean peak radiation power along the length of the device.

In addition to amplifying the short-pulse radiation power to saturation, the second undulator operating to saturation will reduce the peak radiation power fluctuations. The shot-to-shot power fluctuations of the input radiation into the second undulator, Eq. (6), are considerably reduced in the second undulator due to operation in

Table 3. Second Undulator ($L_2 = 51.8 \text{ m}$) Input Electron and Photon-Beam Parameters and Output-Radiation Parameters

Input electron beam:	
Peak current	3.9 kA
Bunch duration, FWHM	200 fs
Uncorrelated energy spread	0.008%
Beam shot-noise power	6.4 kW
Input radiation:	
Pulse duration, FWHM	7.1 fs
Mean peak radiation power	2.5 MW
Bandwidth, FWHM	3.1×10^{-4}
Power fluctuations, rms	37%
Output radiation:	
Pulse duration, FWHM	7.1 fs
Mean peak radiation power	23 GW
Bandwidth, FWHM	3.1×10^{-4}
Power fluctuations, rms	4%
Transverse rms radiation size	31 μm
Transverse rms radiation divergence	0.5 μrad
Mean coherent photons per pulse	4×10^{10}

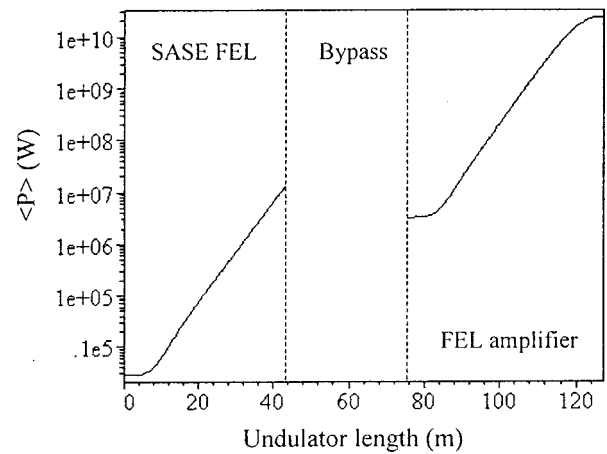


Fig. 5. Mean peak radiation power along length of chirped-beam two-stage FEL.

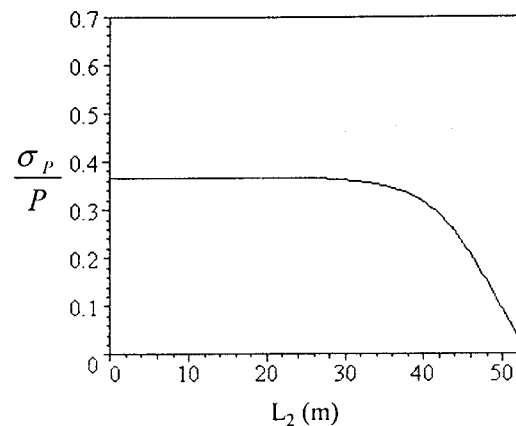


Fig. 6. Radiation power fluctuations along length of second undulator (FEL amplifier).

the nonlinear regime. Figure 6 shows the reduction in relative power fluctuations along the length of the second undulator as the FEL interaction moves into the nonlinear regime of amplification.

The spontaneous emission due to electron-beam shot noise is also amplified in the second undulator. For a second undulator length of $L_2 = 51.8 \text{ m}$, the SASE radiation is amplified to $\langle P_{\text{SASE}}(L_2) \rangle = 0.18 \text{ GW}$, or 0.78% of the peak power in the short-pulse radiation. If this background SASE radiation (noise) is too large for users, then additional monochromators or filters would be necessary to remove the SASE radiation produced in the second undulator.

4. CONCLUSIONS

The chirped-beam two-stage FEL described in this paper has the ability to control the pulse duration of the FEL radiation as well as to stabilize the central radiation frequency. Selection of the radiation by the monochromator also allows the possibility of greatly improved temporal coherence. Seeding the short-duration radiation into a second undulator (FEL amplifier) has several advantages compared with a single undulator (SASE-FEL) followed by x-ray optics. By seeding the radiation into a second undulator, any power loss in the monochromator is recov-

ered in the second undulator, the shot-to-shot radiation-intensity fluctuations are decreased due to operation in the nonlinear regime, and damage to optical elements of the monochromator is reduced since the first undulator terminates before saturation is reached.

In this paper, we have examined a chirped-beam two-stage FEL device based on the present LCLS design parameters. It was shown that such a device is capable of producing high-power ($P_{\text{sat}} \approx 10$ GW) x-ray pulses with femtosecond pulse durations. The requirements of future users of femtosecond x-ray pulses will determine the final selection of parameters for a chirped-beam two-stage FEL.

APPENDIX A

In this appendix, the linear FEL theory is extended to include an electron beam with an energy distribution correlated to the longitudinal position within the beam, and the effects of the energy-chirped electron beam on the evolution of the FEL radiation are investigated. Our approach is to solve the coupled Maxwell–Boltzmann equations in one dimension in the exponential gain regime. It is convenient to define the FEL phase $\theta = k(z - ct) + k_u z$, where $k = 2\pi/\lambda$ and $k_u = 2\pi/\lambda_u$, and to change the independent variables from (z, t) to (θ, z) . The conjugate variable to θ is the energy deviation $\eta = (\gamma - \gamma_0)/\gamma_0$, where γ_0 is the mean electron-beam energy. The equations of motion for each electron in the laser and undulator fields are given by the well-known FEL pendulum equations¹⁰:

$$\dot{\theta} = 2k_u \eta, \quad (9a)$$

$$\dot{\eta} = -\kappa_B a \exp(i\theta), \quad (9b)$$

where $a = [eA/(mc^2)]\exp[-ik(z - ct)]$ is the laser-field envelope (i.e., amplitude of the normalized transverse vector potential of the laser field). The constant in Eq. (9b) is $\kappa_B = ka_u[JJ]/(2\gamma_0^2)$, where $a_u = eB_u/(mc^2k_u)$ is the normalized undulator magnetic field strength and, for a planar undulator, $[JJ] = J_0(\zeta) - J_1(\zeta)$ with $\zeta = \alpha_u^2/(4 + 2\alpha_u^2)$. The dots indicate differentiation with respect to z .

The Maxwell equations can be combined, assuming a slowly varying laser-field envelope, to yield the evolution equation

$$\left(\frac{\partial}{\partial z} + k_u \frac{\partial}{\partial \theta}\right) a = k_M \exp(-i\theta) \int d\eta f, \quad (10)$$

where f is the electron-beam phase-space distribution and $\kappa_M = \omega_p^2 a_u [JJ]/(4c^2 \gamma_0 k)$. Here $\omega_p^2 = 4\pi n e^2/m$ is the plasma frequency of the electron beam with number density n . The constants κ_B and κ_M define the FEL parameter: $\kappa_M \kappa_B = 4k_u^2 \rho^3$.

The phase-space distribution of the electron beam can be expressed as a Klimontovich distribution,^{11,12}

$$f(\theta, \eta, z) = \frac{k}{n\sigma} \sum_j \delta(\theta - \theta_j) \delta(\eta - \eta_j), \quad (11)$$

where σ is the transverse beam area. The electron-beam phase-space distribution satisfies the phase-space continuity equation,

$$\left(\frac{\partial}{\partial z} + \dot{\theta} \frac{\partial}{\partial \theta} + \dot{\eta} \frac{\partial}{\partial \eta}\right) f = 0. \quad (12)$$

We will assume that the normalized laser-field amplitude is in the nonrelativistic regime, i.e., $a \ll 1$. In the exponential gain regime, we can consider the first-order evolution of the electron-beam distribution $f = f_0 + \Delta f_0 + f_1$, where f_0 is the unperturbed distribution ensemble average $\langle f \rangle = f_0$, Δf_0 is the initial fluctuations in the distribution, and f_1 is a small (of the order of the laser amplitude a) perturbation to the distribution. The ensemble average of the unperturbed distribution may be decomposed into $f_0 = \chi(\theta - \dot{\theta}z)V(\theta - \dot{\theta}z, \eta)$, where $\chi(\theta)$ is the initial smooth bunch profile and $V(\theta, \eta)$ is the initial energy spread, which may contain phase dependence (i.e., an energy spread that is correlated to the electron position). Linearizing the Boltzmann equation, Eq. (12) yields

$$\left(\frac{\partial}{\partial z} + \dot{\theta} \frac{\partial}{\partial \theta}\right) f_1 = \kappa_B a \exp(i\theta) \frac{\partial f_0}{\partial \eta}, \quad (13)$$

with the solution for the distribution perturbation

$$f_1 = \kappa_B \exp(i\theta) \frac{\partial f_0}{\partial \eta} \int_0^z dz' \exp[i\dot{\theta}(z' - z)] a(\theta', z'), \quad (14)$$

where $\theta' = \theta - \dot{\theta}(z - z')$.

The coupled linear Maxwell and Boltzmann equations Eqs. (10) and (13) can be solved^{11,12} for the evolution of the laser-field envelope by applying the Laplace transform,

$$\begin{aligned} \alpha(\theta, z) = & \int d\theta' H(\theta - \theta') \int_{L} \frac{ds}{2\pi i} \left[a_0(\theta') \right. \\ & + \frac{\kappa_M}{k_u} \int d\eta \exp(-i\theta') \frac{\Delta f_0}{s + 2i\eta} \Big] \\ & \times \exp \left[s(k_u z - \theta + \theta') \right. \\ & \left. - (2\rho)^3 i \int_{\theta'}^{\theta} d\theta'' \int d\eta \frac{f_0(\theta'', \eta)}{(s + 2i\eta)^2} \right], \quad (15) \end{aligned}$$

where $a_0(\theta) = \alpha(\theta, z = 0)$ is the initial laser-field amplitude, and H is the Heaviside step function. The contour integration in the complex s plane lies to the right of all poles. The FEL radiation intensity is proportional to the ensemble average of the square of the field amplitude,¹³

$$\begin{aligned} \langle a^* a \rangle = & \left| \int d\theta' a_0(\theta') G_{\text{CA}} \right|^2 \\ & + \frac{\kappa_M^2 k}{k_u^2 n \sigma} \int d\theta' \chi(\theta') |G_{\text{SASE}}|^2 \\ & + \frac{\kappa_M^2}{k_u^2} \left| \int d\theta' \chi(\theta') \exp(i\theta') G_{\text{SASE}} \right|^2, \quad (16) \end{aligned}$$

where $G_{\text{SASE}}(\theta, \theta', z)$ and $G_{\text{CA}}(\theta, \theta', z)$ are the Green functions for self-amplified spontaneous emission (SASE) and coherent amplification (CA) respectively. The first term on the right-hand side of Eq. (16) is responsible for the coherent amplification of the initial radiation field in the FEL. The second term of Eq. (16) is the usual incoherent SASE, and the third term is the coherent SASE due to initial bunching of the electron beam at the radiation wavelength. For the case of the chirped-beam two-stage FEL, the incoherent SASE term dominates in the first undulator, and the CA term dominates in the second undulator. The CA term dominates throughout the second undulator because the input radiation power into the second undulator is much greater than the electron-beam shot-noise power (which seeds the incoherent SASE radiation), the bunching at the radiation wavelength responsible for the coherent SASE term is destroyed in the electron-beam bypass, and the second undulator terminates many gain lengths before the saturation of the incoherent SASE radiation.

The Green's function in Eq. (16) is

$$G(\theta, \theta', z) = H(\theta - \theta') \int_{L/2\pi i} \frac{ds}{2\pi i} \exp[s(k_u z - \theta + \theta')] \times \exp\left[-(2\rho)^3 i \int_{\theta'}^{\theta} d\theta'' \int d\eta \frac{f_0(\theta'', \eta)}{(s + 2i\eta)^2}\right] \times \begin{cases} 1 & \text{for CA} \\ \int d\eta \frac{V(\eta, \theta')}{s + 2i\eta} & \text{for SASE} \end{cases} \quad (17)$$

The Green's function vanishes when $\theta - \theta' \geq k_u z$; hence only electrons within one slippage length before θ can contribute to the field at θ . The Green's function can be expressed in the convenient form¹⁴

$$G(\theta, \theta', z) = \int_{-\infty - i\epsilon}^{\infty - i\epsilon} \frac{dq}{2\pi i} \exp[iq(\theta - \theta')] \times \int_{L/2\pi i} \frac{ds}{2\pi i} \frac{\exp(sk_u z)}{D} \times \begin{cases} 1 & \text{for CA} \\ \int d\eta \frac{V(\eta, \theta')}{s + 2i\eta} & \text{for SASE} \end{cases} \quad (18)$$

where ϵ is an infinitesimal positive number, $q = (\omega - \omega_0)/\omega_0$ is the frequency detuning, and D is the generalized dispersion relation for the FEL interaction,

$$D = s + iq - \frac{i(2\rho)^3}{(\theta - \theta')} \int_{\theta'}^{\theta} d\theta'' \int d\eta \frac{f_0(\theta'', \eta)}{(s + 2i\eta)^2}. \quad (19)$$

The roots of the dispersion relation Eq. (19) determine the exponential growth of the Green's function Eq. (18) through the residues of the inverse Laplace contour. Equations (15)–(19) are a generalization of previous 1D FEL theory^{11–14} to include the possibility of an electron beam with an energy distribution correlated to the longitudinal position within the beam.

For the case of a flattop unbunched monoenergetic beam $f_0 = \delta(\eta)$, the generalized dispersion relation Eq. (19) reduces to the usual cubic characteristic equation of 1D FEL theory,³

$$D = s + iq - \frac{i(2\rho)^3}{s^2}. \quad (20)$$

The real part of the fastest growing root of the cubic equation, assuming $q/(2\rho) < 1$, is

$$\text{Re}\left[\frac{s}{2\rho}\right] = \frac{\sqrt{3}}{2} \left[1 - \frac{1}{9} \left(\frac{q}{2\rho}\right)^2\right]. \quad (21)$$

Solving Eq. (18) by use of the fastest growing root Eq. (21) yields the well-known 1D gain length $L_g = 1/(2\sqrt{3}\rho k_u)$ and Gaussian dependence on the frequency detuning, with FEL bandwidth $\sigma_\omega = \omega_0[9\rho/(\sqrt{3}k_u z)]^{1/2}$.

Consider the case of an energy-chirped electron beam $f_0 = \delta(\eta - \hat{\alpha}\theta)$. Here we are considering an energy deviation that is linearly proportional to the FEL phase (longitudinal position within the electron beam) $\eta_j(0) = \alpha\theta_j(0)/(k + k_u)L_b = \hat{\alpha}\theta_j(0)$. For the case of an energy-chirped electron beam, the dispersion relation Eq. (19) is

$$D = s + iq - \frac{i(2\rho)^3}{(s + 2i\hat{\alpha}\theta)(s + 2i\hat{\alpha}\theta')}. \quad (22)$$

Equation (22) reduces to the cubic characteristic equation for an unbunched monoenergetic electron beam [Eq. (20)] if $|2\hat{\alpha}\theta| \ll |s|$. Since $|\theta| \ll |k_u z|$ (i.e., only electrons within one slippage length will contribute), the correction to the FEL dynamics due to the energy chirp will be small if $|\hat{\alpha}k_u z/\rho| \ll |s/2\rho| \sim 1$, or

$$\frac{\alpha}{L_b} \left(\frac{\lambda}{\rho}\right) \ll \rho. \quad (23)$$

Therefore the corrections to the dynamics due to the energy chirp will be small if the energy chirp over one slippage length is much less than the FEL parameter. For LCLS parameters (with 0.5% energy chirp), $\alpha\lambda/(\rho^2 L_b) \sim 10^{-2}$. Assuming that $[\alpha\lambda/(\rho^2 L_b)] \ll 1$, the lowest-order correction to gain length $L_g(\alpha)$ is

$$\frac{L_g(\alpha) - L_g(0)}{L_g(0)} \lesssim \frac{1}{9} \left(\frac{\alpha\lambda}{L_b\rho^2}\right)^2, \quad (24)$$

where $L_g(0) = 1/(2k_u\rho\sqrt{3})$ is the 1D gain length for an unchirped electron beam.

ACKNOWLEDGMENTS

C. B. Schroeder wishes to thank Z. Huang and H.-D. Nuhn for useful discussions. This study was supported by the U.S. Department of Energy, under grant DE-FG03-92ER40693.

*Present address: Lawrence Berkeley National Laboratory, University of California, Berkeley, California 94720.

REFERENCES

1. J. B. Murphy and C. Pellegrini, "Generation of high-intensity coherent radiation in the soft-x-ray and vacuum-ultraviolet region," *J. Opt. Soc. Am. B* **2**, 259–264 (1985).
2. J. Arthur *et al.*, "Linac Coherent Light Source (LCLS) conceptual design report," Stanford Linear Accelerator Center Report SLAC-R-593 (Stanford University, Stanford, Calif., 2002).
3. R. Bonifacio, L. De Salvo, T. Pierini, N. Piovella, and C. Pellegrini, "Spectrum, temporal structure, and fluctuations in a high-gain free-electron laser starting from noise," *Phys. Rev. Lett.* **73**, 70–73 (1994).
4. C. Pellegrini, "High power femtosecond pulses from an X-ray SASE-FEL," *Nucl. Instrum. Methods Phys. Res. A* **445**, 124–127 (2000).
5. J. Feldhaus, E. L. Saldin, J. R. Schneider, E. A. Schneidmiller, and M. V. Yurkov, "Possible application of X-ray optical elements for reducing the spectral bandwidth of an X-ray SASE FEL," *Opt. Commun.* **140**, 341–352 (1997).
6. E. Saldin, E. A. Schneidmiller, and M. V. Yurkov, "Optimization of a seeding option for the VUV free electron laser at DESY," *Nucl. Instrum. Methods Phys. Res. A* **445**, 178–182 (2000).
7. E. L. Saldin, E. A. Schneidmiller, and M. V. Yurkov, "Statistical properties of radiation from VUV and X-ray free electron laser," *Opt. Commun.* **148**, 383–403 (1998).
8. J. Goodman, *Statistical Optics* (Wiley, New York, 1985).
9. S. Reiche, "GENESIS 1.3: a fully 3D time-dependent FEL simulation code," *Nucl. Instrum. Methods Phys. Res. A* **429**, 243–248 (1999).
10. For a review, see J. B. Murphy and C. Pellegrini, "Introduction to the physics of free-electron lasers," in *Laser Handbook*, W. B. Colson, C. Pellegrini, and A. Renieri, eds. (North-Holland, Amsterdam, 1990), Vol. 6.
11. K.-J. Kim, "An analysis of self-amplified spontaneous emission," *Nucl. Instrum. Methods Phys. Res. A* **250**, 396–403 (1986).
12. K.-J. Kim and S. J. Hahn, "Finite pulse effects in self-amplified-spontaneous-emission," *Nucl. Instrum. Methods Phys. Res. A* **358**, 93–95 (1995).
13. Z. Huang and K.-J. Kim, "Effects of bunch density gradient in high-gain free-electron lasers," *Nucl. Instrum. Methods Phys. Res. A* **445**, 105–109 (2000).
14. S. Krinsky, "Transient analysis of free-electron lasers with discrete radiators," *Phys. Rev. E* **59**, 1171–1183 (1999).